Nanoscale internally referenced oxygen sensors produced from self-assembled nanofilms on fluorescent nanoparticles

Kyle B. Guice
Louisiana Tech University
Chemical Engineering
and
Institute for Micromanufacturing
911 Hergot St.
Ruston, Louisiana 71272

Mary E. Caldorera
Michael J. McShane
Louisiana Tech University
Biomedical Engineering
and
Institute for Micromanufacturing
911 Hergot St.
Ruston, Louisiana 71272
E-mail: mcshane@latech.edu

Abstract. A novel sensor fabrication concept using indicators trapped in nanoengineered ultrathin films deposited on fluorescent nanoparticles is demonstrated for oxygen sensing. The nanoscale systems are based on the quenching of *tris*(4,7-diphenyl-1,10-phenanthroline)ruthenium(II) immobilized within polyelectrolyte multilayers deposited on the surface of nanoparticle templates. The ionically bound nanofilms create a porous scaffold into which controlled precipitation of the chromophore is achieved using a combination of electrostatic attraction and dye insolubility in water. The fluorescent nanoparticles act as physical scaffolds and also provide a complementary spectral signature for use as an internal intensity reference. Oxygen sensors created on 100-nm yellow-green fluorescent particles exhibit a linear Stern-Volmer behavior with a quenching constant of 1.06/mM and sensitivity of 60%, which demonstrates that the dye is still partially accessible to oxygen following immobilization. To demonstrate the feasibility of intracellular metabolic monitoring with such nanoprobes, the oxygen sensors were chemically delivered into human dermal fibroblasts with no apparent loss in cell viability. The results prove that the approach to sensor production is facile and leads to sensitive systems that can be further optimized for improved response, and these findings support the further development of similar self-referenced probes toward quantitative intracellular analysis.
[DOI: 10.1117/1.2147419]

Keywords: nanosensors; quenching; layer-by-layer self-assembly; intracellular monitoring.

Paper 04104RRR received Jun. 21, 2004; revised manuscript received Aug. 5, 2005; accepted for publication Aug. 8, 2005; published online Dec. 29, 2005.

1 Introduction

Fluorescence sensing is advantageous in analyte detection schemes where high sensitivity or remote detection is required.[1] The high sensitivity and analyte specificity of fluorescence sensing makes the method particularly useful in biological analysis. However, dye toxicity, compartmentalization in cells, diffusion-induced dye loss, and biofouling limit the practical sensing lifetime of dye in solution and often distort calibrations developed under different conditions.[2] Therefore, a method for the immobilization of sensor components that protects both the sensing chemistry from the biology and the biology from the sensing chemistry is desirable for long-term monitoring *in vitro* or *in vivo*. It is also advantageous to incorporate a second dye, insensitive to the target analyte, into the system to correct for nonspecific signal modulation.

Encapsulation techniques involving dialysis membranes,[3] liposomes,[4] or polymer or silica matrices[2,5–8] have been previously reported for sensor chemistry. Liposomal packaging, while suitable for delivery of naked dye or DNA to interior of cells, generally is not considered as a stable long-term solution for immobilization that is appropriate for sensor applications. For the polymer and sol-gel approaches, immobilization often involves performing fairly complex chemical reactions in microemulsions to achieve the desired size, plus determining a method for loading of dye. Furthermore, coimmobilization of multiple types of dye molecules adds a degree of difficulty since methods must be developed to immobilize both dyes in specific proportion. Stoichiometrically mixing materials can easily give a ratiometric assay in solution; however, immobilization in a matrix does not necessarily follow directly from solution phase, depending on the immobilization process used. Coimmobilization is complicated by different solubilities and partition coefficients for dyes. The primary examples of successful ratiometric optical nanoprobe production are the PEBBLES (probes encapsulated by biologically localized embedding),[5–7] for which a number of demonstrations for oxygen sensors have been reported.[9,10]

Address all correspondence to Michael J. McShane, Louisiana Tech University, Biomedical Engineering and Institute for Micromanufacturing, 911 Hergot St., Ruston, Louisiana 71272. Tel.: 318–257–5100; Fax: 318–257–5104; E-mail: mcshane@latech.edu

1083-3668/2005/10(6)/064031/10/$22.00 © 2005 SPIE

A novel alternative to coimmobilization of sensor materials involves multistep assembly using nanoengineering techniques. One example of this involves the utilization of fluorescent nanoparticles as templates for precise deposition of indicator molecules. These particles can be used both as a carrier for sensor chemistry as well as an internal intensity reference, due to their inert fluorescence, as long as the spectral properties are chosen to be appropriately complementary to the indicator. Fortunately, fluorescent templates can be produced with a variety of spectral properties to accommodate fluorescent indicator constraints. Therefore, a key challenge is the identification of a suitable technique to deposit the indicator molecules onto the reference nanotemplate in a controllable manner such that the desired spectral feature, an emission spectrum exhibiting two distinct peaks resulting from excitation by a single source, can be obtained with a high degree of control.

Formation of tailored thin films on charged surfaces via layer-by-layer (LbL) self-assembly is an emerging method for the fabrication of micro/nanostructures with controllable properties.[11–13] Fundamental research has shown that layers of oppositely charged macromolecules can be stacked with nanometer precision, and film properties can be controlled using multiple methods.[14,15] While initial research involved planar templates, the LbL process has been employed in the fabrication of 3-D structures by use of charged micro/nanoparticles as templates.[16–18] A potentially significant application of LbL techniques involves the fabrication of fluorescence-based micro/nanosensors.[19]

Methods of LbL to immobilize fluorescent probes in planar films,[20] microparticle-based films,[21] and microcapsules[22,23] and nanocapsules[19] have been investigated. Techniques that have been utilized for the localization of low molecular weight fluorescent indicators within ultrathin films include direct assembly,[21,24,25] premixing,[21,26] pH-assisted adsorption,[23,24] and covalent linkage to polyelectrolytes.[21,25] These investigations have demonstrated that specific dyes remain immobilized and maintain sensing properties when embedded in LbL films or encapsulated within LbL capsules. However, no generalized method for dye immobilization has yet been proposed.

To address this issue, a novel technique for fluorescence sensor fabrication was developed for the purpose of creating oxygen-sensitive nanoparticles. Local oxygen concentration and oxygen consumption rates are critical factors in cell growth rates.[27,28] Several oxygen-sensitive molecules are known, particularly metal-ligand complexes (MLCs) that are quenched by oxygen.[1] Of these, the ruthenium-based compounds are the most widely used; in general, they have acceptable photostability, a large Stokes shift, and long lifetimes, of the order of microseconds,[29] conferring the oxygen-sensitive property due to collisional quenching. The large Stokes shifts typically associated with the compounds reduce excitation interference in emission-based sensors, and the long lifetimes improve sensitivity to oxygen, thus improving sensor resolution. Dichloride ruthenium compounds, such as *tris*(4,7-diphenyl-1,10-phenanthroline)ruthenium(II) dichloride ($[Ru(Ph_2phen)_3]Cl_2$), offer higher oxygen-quenching sensitivities than other ruthenium compounds.[29,30] The properties of ($[Ru(Ph_2phen)3]Cl_2$) have been widely analyzed in solution and in polymer and silica supports,[31–34] and a two-state Stern-Volmer model has been developed to describe the quenching behavior of $[Ru(Ph_2phen)_3]^{2+}$ by oxygen.[29] Ruthenium-doped silica nanoparticles have previously been investigated as biomarkers for human leukemia cells,[8] but without a second fluorophore acting as an internal reference, such systems cannot be used for quantitative analysis.

It is notable that a previous report presented successful ratiometric oxygen sensor production using polyelectrolyte microcapsules,[23] though these systems exhibited some drawbacks that make them unsuitable for intracellular deployment. First, the large size capsules (5 μm) were not amenable to endocytotic uptake or intracellular delivery, and these capsules are increasingly difficult to produce with decreasing size. Second, a different ligand was used in that case (bipyridyl), which made the dye more water soluble (harder to stably immobilize) and less sensitive to oxygen. Therefore, a different approach was taken to realize nanosensors more appropriate for intracellular measurements.

In this paper, a novel, facile, and repeatable procedure to create nanoscale systems for fluorescence sensing is described. Fluorescent nanoparticles with spectral properties similar to fluorescein (λ_{ex}=460 nm, λ_{em}=515 nm) were used as the template for fluorescent sensors for the detection of oxygen based on the quenching of a long-lifetime ruthenium compound. The size of the templates chosen was 100 nm, which is an appropriate scale for intracellular analysis.[5] Dye adsorption into LbL films was accomplished using insolubility-induced precipitation in water.[35] Following fabrication, the sensors were characterized to determine oxygen sensitivity, and then were delivered to the interior of living cells in culture for analysis of distribution and toxicity. Such sensors capable of detecting changes in oxygen concentration are useful not only in oxygen detection schemes, but also in schemes that utilize oxygen changes as an indirect method to quantify other species,[36–38] such as enzymatic reactions wherein oxygen is a cosubstrate or product. More importantly, the general sensor development procedure described here is more broadly applicable, enabling fabrication of sensors for other targets using similar methods.

2 Experimental Methods

2.1 *Materials*

Carboxylate-modified FluoSpheres® [100-nm, yellow-green (λ_{ex}=488 nm, λ_{em}=515 nm), 2% solids] were obtained from Molecular Probes. Poly(styrene sulfonic acid) sodium salt [PSS, molecular weight (MW) ~ 1 MDal, Sigma) and poly(allylamine hydrochloride) (PAH, MW ~ 200 kDal, Sigma) were used in polyelectrolyte film formation. Separate solutions of PAH and PSS (2 mg/mL, 0.1-MKCl) were prepared from deionized water and stored at room temperature. *Tris*(4,7-diphenyl-1,10-phenanthroline)ruthenium(II) dichloride ($[Ru(Ph_2phen)_3Cl_2]$, MW=1169, Fluka) was used as the oxygen-sensitive fluorophore. The molecular structure of the dissociated sensing cation $[Ru(Ph_2phen)_3]^{2+}$ is shown in Fig. 1. $[Ru(Ph_2phen)_3Cl_2]$ was dissolved in a 0.11-mM stock solution (37% methanol, 63% deionized water by volume) containing 6.67-mM NaOH.

Poly(ethyleneimine) (PEI, MW ~ 750 kDal, Sigma) was dissolved (2 mg/mL) in type I water for use in delivery studies. Human dermal fibroblasts (HDFs) were obtained from

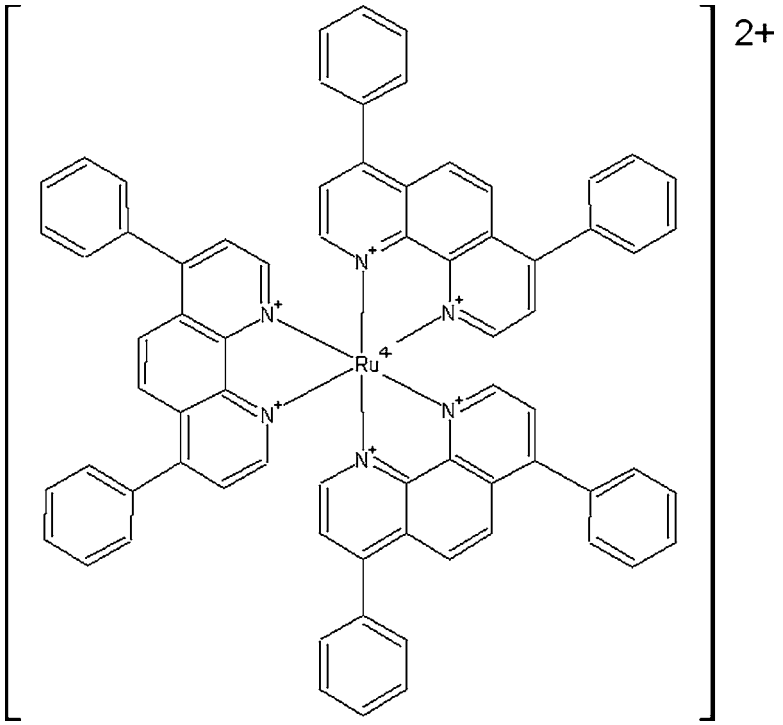

Fig. 1 Molecular structure of *tris*(4,7-diphenyl-1,10-phenanthroline)ruthenium(II) $[Ru(Ph_2phen)_3]^{2+}$ (dissociated form of dichloride salt).

Cascade Biologics. Growth media [Dulbecco's minimum essential medium (DMEM), low glucose] and fetal bovine serum (FBS) were obtained from Atlanta Biologicals. Plastic microplates (96 wells) were obtained from Fisher Scientific. Hank's balanced salt solution (HBSS) was obtained from Sigma in powder form and dissolved in type I water.

2.2 *Characterization of* $[Ru(Ph_2phen)_3]^{2+}$ *Adsorption on Quartz Crystal Microbalance (QCM) Templates*

To analyze dye uptake using the insolubility-induced precipitation technique, multilayer films were fabricated on QCM resonators using standard methods.[7] Alternate PAH/PSS adsorption cycles were monitored using QCM analysis with resonators having evaporated silver electrodes with combined surface area of $0.16\,cm^2$ and initial resonance frequency of 9 MHz (AT-cut, Sanwa Tsusho). During the assembly procedure, each resonator was dipped into the cleaning solution [39% EtOH, 1% KOH, 60% deionized (DI) water] and sonicated in a Branson 1510 ultrasonic bath to create a negative surface charge on the resonator. The resonator was then immersed in a polyelectrolyte solution for 15 min to allow complete surface saturation, rinsed twice by immersion in water, and dried with streaming nitrogen. The resonance frequency was then measured using a USI SC-7201 frequency counter. Films with architectures ranging from $\{PAH/PSS\}_1$ to $\{PAH/PSS\}_5$ were deposited on different QCM resonators. The subscripts 1 and 5 represent the number of bilayers of PAH/PSS deposited. To assess the influence of surface-charge on the immobilization process, films with architectures of $\{PAH/PSS\}_1PAH$ to $\{PAH/PSS\}_5PAH$ were also deposited on QCM resonators. A control sample, with no polyelectrolyte multilayers, was also analyzed. For $[Ru(Ph_2phen)_3]^{2+}$ adsorption, the resonator was immersed in dye stock solution for 30 min. The change in mass due to deposition the final polyelectrolyte layer was determined using the frequency counter.

2.3 *Characterization of* $[Ru(Ph_2phen)_3]^{2+}$ *Adsorption on FluoSpheres®*

Films with architecture $\{PAH/PSS\}_3$ were constructed on fluorescent nanoparticle templates using standard methods.[16] Initially, 40 μL of nanoparticles ($\sim 1.5\times10^{15}$ particles) was used for coating. The LbL assembly process for deposition of ultrathin films on nanoparticles is shown in Fig. 2. The nanoparticles were suspended alternatively in 1 mL of PAH and PSS solutions for 20-min intervals, with three standard rinse cycles in DI water between each polyelectrolyte step. Standard rinse cycles included centrifugation at 13,000 rpm for 1 h in an Eppendorf 5804R centrifuge and sonication for 1 min. After each layer was deposited, a 10-μL sample of the 1-mL volume of coated nanoparticles was diluted in 2 mL DI water, and the surface potential of the modified particles was measured using the ZetaPlus ζ-potential analyzer (Brookhaven Instruments). Once the desired film architecture was attained, a total of three bilayers of {PAH/PSS}, the nanoparticles were suspended in 1 mL of $[Ru(Ph_2phen)_3]^{2+}$ stock solution for 24 h. Following this period the nanoparticles were rinsed three times in DI water.

To determine the total mass of $[Ru(Ph_2phen)_3]^{2+}$ adsorbed into the polyelectrolyte multilayer films on nanoparticles, the concentration of removed $[Ru(Ph_2phen)_3Cl_2]$ supernatant was determined using a premeasured absorbance calibration curve. The sample was irradiated using an Ocean Optics LS-1 tungsten halogen lamp, and absorbance data were collected for the diluted supernatant using an Ocean Optics USB2000

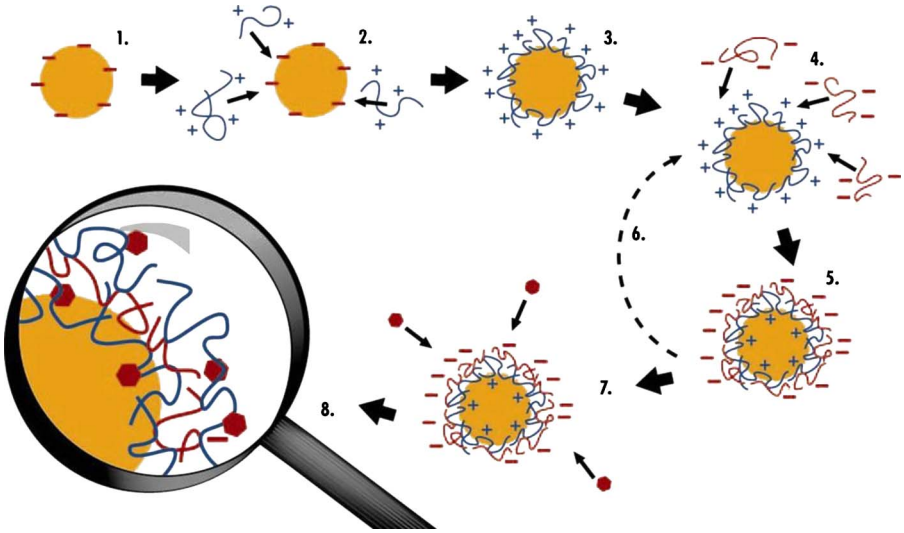

Fig. 2 Schematic for sensor production process. Ultrathin films are deposited on 100-nm fluorescent templates using L & L assembly. $[Ru(Ph_2phen)_3]^{2+}$ precipitation into the nanofilms is shown as the final step in sensor fabrication.

spectrophotometer. The absorbance at 463 nm was plotted against a $[Ru(Ph_2phen)_3]^{2+}$ absorbance-concentration profile, obtained through successive dilution of the stock $[Ru(Ph_2phen)_3Cl_2]$ solution, and the concentration of $[Ru(Ph_2phen)_3Cl_2]$ in the final supernatant was determined. The removed supernatant concentration was subtracted from the loading solution concentration to determine the mass of $[Ru(Ph_2phen)_3]^{2+}$ adsorbed.

To assess the stability of the immobilized dye-nanoparticle system, absorbance data for supernatant of the nanosensor suspension were collected over a 28-day period following O_2 studies. This was performed to determine the amount of indicator released from the nanofilms under normal conditions of wet storage or use in aqueous media. The nanosensor solution was centrifuged and the supernatant was removed four times during the 4-week period for absorbance studies. The supernatant absorbance data were collected and compared to the absorbance of the original suspension.

2.4 *Characterization of Sensor Response to Changes in Bulk Oxygen Concentration*

To determine the response of the $[Ru(Ph_2phen)_3]^{2+}$-nanoparticle sensors to changes in O_2 concentration, the final suspension of nanosensors (in 2 mL DI water) was placed in a cuvette into which O_2 and N_2 were bubbled into the chamber at random concentrations using individual regulators. To minimize time-correlated nonspecific effects, O_2 concentrations were adjusted alternatively higher or lower for each successive measurement. Oxygen measurements were collected from a Unisense PA2000 picoammeter with an OX500 micro-oxygen electrode connected to a PC running LABVIEW with a data acquisition (DAQ) card. An Hg-lamp with a 460-nm emission filter was used to excite the nanosensors using a fiber probe; emission spectra were collected with a fiber probe oriented perpendicularly to the excitation probe, and the spectra were analyzed using an Ocean Optics spectrometer. Three spectra were collected for each oxygen concentration, and the data were averaged and normalized to the maximum peak for green emission (515 nm). The normalized fluorescence intensity at 614 nm was used as the ratiometric indicator of oxygen.

A similar experiment was performed to evaluate the susceptibility of the sensors to interference by proteins or peptides in the surrounding solution, as might be encountered in the cytosol. Using a separate batch of sensors, which were produced using different loading conditions (ruthenium to nanoparticle concentration) and were stored wet (in DI water) for >10 months, sensors were split into separate cuvettes for comparison experiments. Both samples initially comprised nanosensors in DI water, while poly(L-lysine) (PLL) and FBS were added to the second and third samples. For five different oxygen concentrations ranging from 0 to 100%, spectra were measured (three at each concentration), and Stern-Volmer curves were constructed to determine whether the presence of protein and/or peptide resulted in significantly different quenching
behavior.

2.5 *Intracellular Delivery*

Sensors were produced as described above, using sterilized water and materials, and all procedures were performed under a laminar flow hood. Human dermal fibroblasts (passage six) were cultured in 96-well plates using DMEM supplemented with 10% FBS (V/V). The $[Ru(Ph_2phen)_3]^{2+}$-nanoparticle sensors were coated with PEI, a cationic polymer frequently used to complex with DNA for transfection, using electrostatic adsorption. PEI-coated sensors suspended in sterilized type I water were added directly to cells preplated and adhered onto 96-well plates. Based on previously reported methods,[39] the total number of particles added to each well was varied from 10^8 to 10^{10}. After 48-h exposure to PEI-coated nanoparticles, cells were rinsed with HBSS, and media was reintroduced before imaging with a Leica TCS SP2 laser scanning confocal microscope. Nomarski phase and fluorescence images were collected for the same focal plane to en-

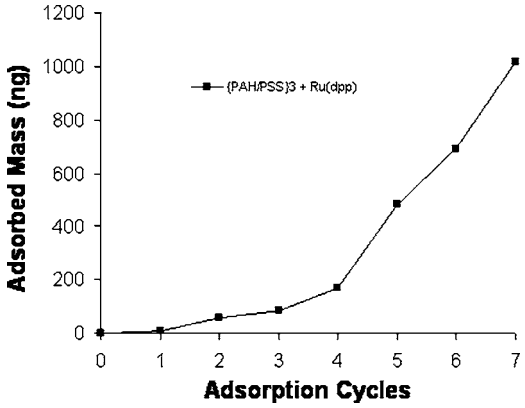

Fig. 3 Growth of $\{PAH/PSS\}_3$ film and $[Ru(Ph_2phen)_3]^{2+}$ adsorption during QCM experiments, with thickness estimated from mass measurements.

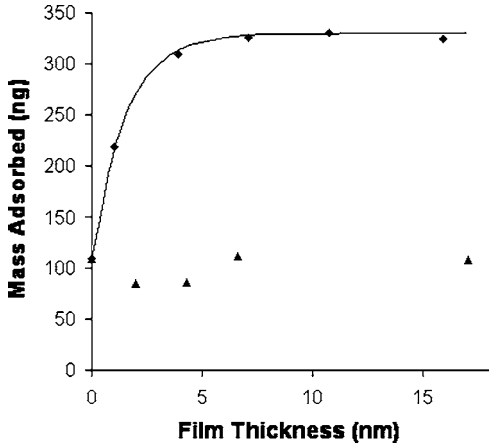

Fig. 4 Mass of $[Ru(Ph_2phen)_3]^{2+}$ adsorbed as an exponential function of film thickness (estimated from mass measurements). The amount of $[Ru(Ph_2phen)_3]^{2+}$ deposited is shown for both PSS-terminal (♦) and PAH-terminal (▲) nanofilms with different numbers of layers.

able coregistration of cellular boundaries and nanoparticle localization.

3 Results and Discussion

3.1 *Mass Deposition Measured as Adsorption onto QCM Resonators*

Mass deposited as a function of layer number for the $\{PAH/PSS\}_3$ QCM sample is shown in Fig. 3. A slower rate of film growth is observed for the first two bilayers, which is in agreement with previous reports.[40] An increase in mass and, therefore, film thickness during the assembly process is evident, with near-linear film growth for the phase after two bilayers. QCM data from other film architectures were observed to show similar trends. The mass increase associated with the $[Ru(Ph_2phen)_3]^{2+}$ adsorption step is also shown in the graph (adsorption cycle 7), though this cannot necessarily be related to a thickness increase due to the penetration of the small molecules into the preadsorbed films.

Measured mass of $[Ru(Ph_2phen)_3]^{2+}$ adsorbed as a function of film thickness (estimated from adsorbed polyelectrolyte mass using the Sauerbrey equation) is shown in Fig. 4. $[Ru(Ph_2phen)_3]^{2+}$ adsorption was measurable on the control sample (resonator without film) and samples with a PAH terminal layer. This suggests that some $[Ru(Ph_2phen)_3]^{2+}$ precipitates directly onto the surface of the crystal. However, $[Ru(Ph_2phen)_3]^{2+}$ adsorption increased threefold in PSS-terminated films of greater than 5 nm thickness. These findings suggest that $[Ru(Ph_2phen)_3]^{2+}$ adsorption into negatively charged films is an exponential function of film thickness. The data were fit to an exponential relationship using an equation of the form

$$M(t) = a(b - e^{-ct}), \tag{1}$$

where M represents the adsorbed mass of $[Ru(Ph_2phen)_3]^{2+}$ (innanograms); t represents the thickness (in nanometers) of the polyelectrolyte film on the surface to which the dye is exposed; and a, b, and c represent adsorption parameters. The calculated coefficient of determination ($R^2=0.998$) indicates that the exponential association is a good fit for the adsorption data. The exponential adsorption function ($a=220\pm15\text{ng}$; $b=1.5\pm0.19$; $c=0.66\pm0.13\text{nm}^{-1}$, 95% confidence) is shown as a line in Fig. 4, which demonstrates excellent fitting. This relationship was found to be consistent for films of identical compositions and assembled using the same conditions.

In contrast to this exponential relationship observed for PSS-terminated polyelectrolyte nanofilms, negligible changes in mass of dye adsorbed relative to the control sample were measured for films terminated with PAH, regardless of the number of polyelectrolyte layers deposited. This indicates that the use of PAH as a terminal layer serves to limit rather than promote $[Ru(Ph_2phen)_3]^{2+}$ adsorption. Poor adsorption of another ruthenium compound into PAH-terminated films was also reported previously.[23] Poor adsorption is likely caused either by surface-charge or water-affinity differences between the terminal polyelectrolytes.

$[Ru(Ph_2phen)_3]^{2+}$ adsorption in films fabricated using LbL assembly is attributable to a difference in water concentration between the stock $[Ru(Ph_2phen)_3Cl_2]$ solution and the $\{PAH/PSS\}_n$ film. As $[Ru(Ph_2phen)_3]^{2+}$ passes through the film, it is immobilized within it. Farhat et al. also studied water concentration in films,[41] and Radtchenko et al. showed that polyelectrolytes used in LbL assembly promote high local water concentrations in films even in near-100% acetone solutions.[35] This is likely due to the presence of the less hydrophobic polyelectrolyte PSS.

The maximum mass of $[Ru(Ph_2phen)_3]^{2+}$ adsorbed to the coated QCM resonator is 330 ng, which is approached as film thickness approaches infinity (Fig. 4). Translated into a depth limitation for adsorption (penetration of the dye into the films), the data suggest that $[Ru(Ph_2phen)_3]^{2+}$ adsorption is highly controllable within 10 nm. Tedeschi et al.[24] reported a depth limitation for adsorption of an anionic pyrene chromophore (4-PSA) to be 17 nm. Differences in depth limitations result from different molecule sizes, different methods of adsorption, or different film compositions. Thus, further control may be easily added by working with alternate materials for the nanofilms, and development of this capability will be a subject of future study.

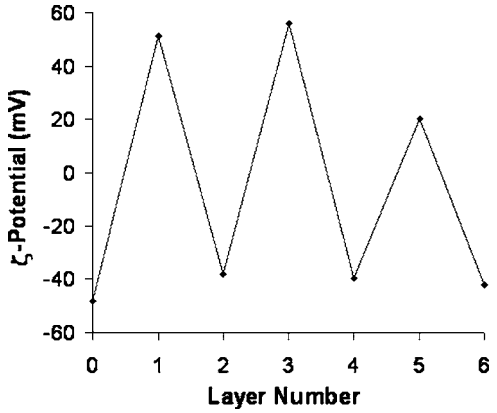

Fig. 5 Zeta potential of polyelectrolyte multilayer films on nanoparticles, as measured during the coating process.

3.2 *Adsorption onto Nanofilm-Coated* FluoSpheres®

Zeta potential as a function of polyion bilayer number for negatively charged nanoparticles alternatively coated with PAH and PSS is shown in Fig. 5. After deposition of each consecutive polyelectrolyte layer, the measured voltage reverses direction. This voltage reversal implies a reversal of surface charge. These results, combined with QCM assembly data, verify that films were formed on the surfaces of the nanoparticles. No quantitative conclusions are made from the zeta potential data.

After 24 h of $[Ru(Ph_2phen)_3]^{2+}$ adsorption, only 4.2% of the original $[Ru(Ph_2phen)_3Cl_2]$ remained in the solution, with the balance immobilized within the multilayers. Assuming no loss of nanoparticles, this translates into an effective $[Ru(Ph_2phen)_3]^{2+}$ concentration within films of approximately 1.2 mg/mL, or six times the $[Ru(Ph_2phen)_3]^{2+}$ concentration of the original $[Ru(Ph_2phen)_3Cl_2]$ solution. Taking into account nanoparticle losses during the coating and rinsing process, the $[Ru(Ph_2phen)_3]^{2+}$ density in films on nanoparticles is much higher.

Nanoparticles with $[Ru(Ph_2phen)_3]^{2+}$ adsorbed into multilayer films were analyzed using a transmission electron microscope (TEM) to assess dye immobilization. A TEM image of several nanoparticle sensors is shown in Fig. 6. After $[Ru(Ph_2phen)_3]^{2+}$ adsorption, the nanoparticles appear round. The TEM results verify that dye adsorption does not produce surface abnormalities, suggesting that the polyelectrolyte films and dye adsorb uniformly over the surface of the nanoparticles.

Absorbance data for the storage supernatant of the nanosensors indicate less than 5% loss of $[Ru(Ph_2phen)_3]^{2+}$ over a 28-day of storage period in DI water. Furthermore, sensors that were rinsed once following 28 days of storage were then stored wet for 9 additional months, and the ruthenium absorbance in the supernatant at the end of that period was negligible. These findings suggest that $[Ru(Ph_2phen)_3]^{2+}$-nanoparticle nanosensors will not lose significant levels of dye during short-term use, such that ratiometric experimental observations should be reliable and should not be expected to have significant adverse effect on cells. Furthermore, the sensors have a long shelf life and can therefore be made in large quantities to be used at a later time.

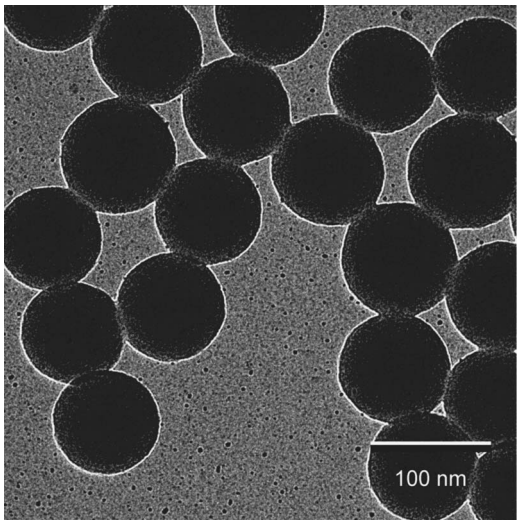

Fig. 6 TEM image of nanoparticles with $[Ru(Ph_2phen)_3]^{2+}$ adsorbed into surface coatings of multilayer nanofilms.

3.3 *Sensor Response to Changes in Bulk Oxygen Concentration*

Normalized $[Ru(Ph_2phen)_3]^{2+}$-nanoparticle spectra at several O_2 concentrations collected during O_2 sensitivity experiments are shown in Fig. 7(a). The top spectrum was collected at 0% O_2, the bottom spectrum was collected at 100% O_2, and the middle spectra were collected at intermediate O_2 concentrations. $[Ru(Ph_2phen)_3]^{2+}$ is quenched in the presence of molecular oxygen, so lower relative $[Ru(Ph_2phen)_3]^{2+}$ fluorescence is expected at higher O_2 concentrations. The figure reveals that the relative intensity of $[Ru(Ph_2phen)_3]^{2+}$ decreases with increasing concentration of dissolved O_2. The $[Ru(Ph_2phen)_3]^{2+}$ in the sample was quenched by approximately 50% from 0% O_2 to 100% O_2. Figure 7(b) is a plot of relative $[Ru(Ph_2phen)_3]^{2+}$ fluorescence (614 nm) versus oxygen concentration, as determined using the micro-oxygen electrode.

The sensitivity of the nanoparticles to oxygen can be computed using the equation

$$S = \frac{(F_0 - F_{\max})}{F_0} \times 100(\%), \tag{2}$$

where F_0 and $F_{\max}$ are intensities at 614 nm, normalized to the emission intensity at 515 nm, F_0 is the relative intensity at zero oxygen concentration, and $F_{\max}$ is the relative intensity under oxygen-saturated conditions. For the sensors tested, the average sensitivity was calculated to be approximately $S = 45\%$. Compared to other sensors based on this metal-ligand complex, this sensitivity is higher $(1.5\times)$ than organically modified silica (ormosil) film matrix,[42] but lower than ormosil and silica nanoparticles[4,43] (56 to 80%).

It is well known that the environment of the dye determines the response behavior, and it is possible that the sensitivity of these systems could be increased by using alternate polyelectrolyte in the films used to adsorb the dye. In addition, photostability depends greatly on the immobilization matrix; it is believed that "caging" (local trapping by the support

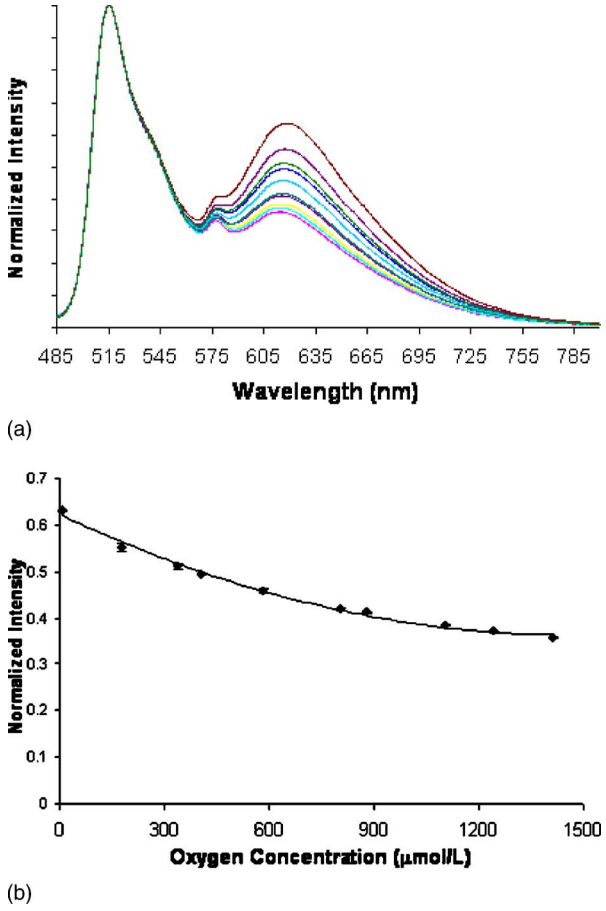

Fig. 7 Results of O_2 sensitivity experiment: (a) normalized fluorescence spectra (λ_{ex}=460 nm) for varying O_2 concentration and (b) normalized $[Ru(Ph_2phen)_3]^{2+}$ emission as a decreasing function of O_2 concentration. Error bars denote one standard deviation for three measurements.

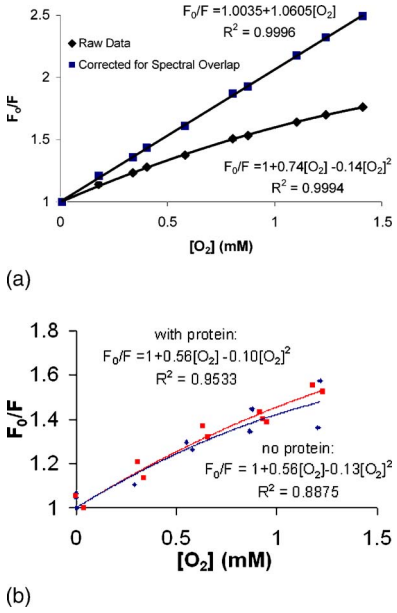

Fig. 8 Stern-Volmer plot for $[Ru(Ph_2phen)_3]^{2+}$ quenching in $\{PAH/PSS\}_3$ films on nanoparticles, where F_0/F refers to the division of the fluorescence intensity ratio (indicator/reference) in the absence of oxygen (F_0) by the fluorescence intensity ratio at the given oxygen concentration. (a) Raw values and values computed after compensating for spectral overlap. The lines denote second-order polynomial (raw data) and linear (corrected data) fits. Error bars denote one standard deviation of three measurements at each concentration. (b) Stern-Volmer plots for nanosensors with and without ambient proteins, using raw data. Equations are second-order polynomial fits.

material) of the highly reactive singlet oxygen produced in the quenching reaction may increase photooxidative degradation rates of the ground-state metal-ligand complexes.[44] Thus, matrices that allow access of solvent molecules to the complexes generally promote greater stability, and it is logical to predict that the nanofilm-based metal complex entrapment methods may lower photobleaching rates due to short diffusion lengths. Measurements of photobleaching using a fluorescence microscope to illuminate nanosensors with 173-μW excitation light for 1 h showed less than 0.5% change in average fluorescence intensity ratio, suggesting that photobleaching of the sensors will be minimal for the intended application. Note also that the nanofilm properties can also be tailored through selection of materials and assembly conditions, leading to differing solvent and oxygen transport properties, which will affect both sensitivity and photodegradation. Furthermore, as recent reports have shown, additional improvements in sensitivity can be gained by moving to alternative long-lifetime materials such as platinum-based complexes.[10] These strategies will be employed in future studies using the facile approach to sensor production.

The modified Stern-Volmer plot for ratiometric data is given in Fig. 8(a), where F_0 and F are intensities at 614 nm, normalized to the emission intensity at 515 nm (F_0 is the relative intensity at zero oxygen concentration). The profile exhibits downward curvature, which matched well with a second-order polynomial (R^2=0.9994), as shown in the figure, where Q is the concentration of O_2. For these data, a first-order quenching constant (A) of 0.74/mM, or 0.0128/Torr, was computed; this linear slope matches well with published values for $[Ru(Ph_2phen)_3]^{2+}$ as oxygen sensors.[30,45] However, the downward-curved shape of the Stern-Volmer plot proves that the indicator response deviates from an ideal single-state system. This type of behavior can be attributed to several factors, including spectral overlap between the emission of reference and indicator and possibly two populations of fluorophores with differing quenching constants. The first possibility, spectral overlap, can be minimized by mathematical correction of the ratio calculation or spectral deconvolution (e.g., principal component analysis) using the pure spectra of the two fluorophores. These are not complicated steps, but do require additional postexperiment processing that is not conducive to direct, real-time measurements.

Investigation of the optical properties of the system revealed spectral overlap with the ruthenium emission from both the yellow/green fluorescent nanoparticle emission as well as a small contribution from to the arc lamp due to the fiber optic sampling system that collects significant reflected light (this is noticeable from a small peak appearing at 575 nm in the measured fluorescence emission spectrum). The normalized value of this offset at 614 nm was calculated to be 17.5% of the fluosphere intensity at 515 nm. In contrast,

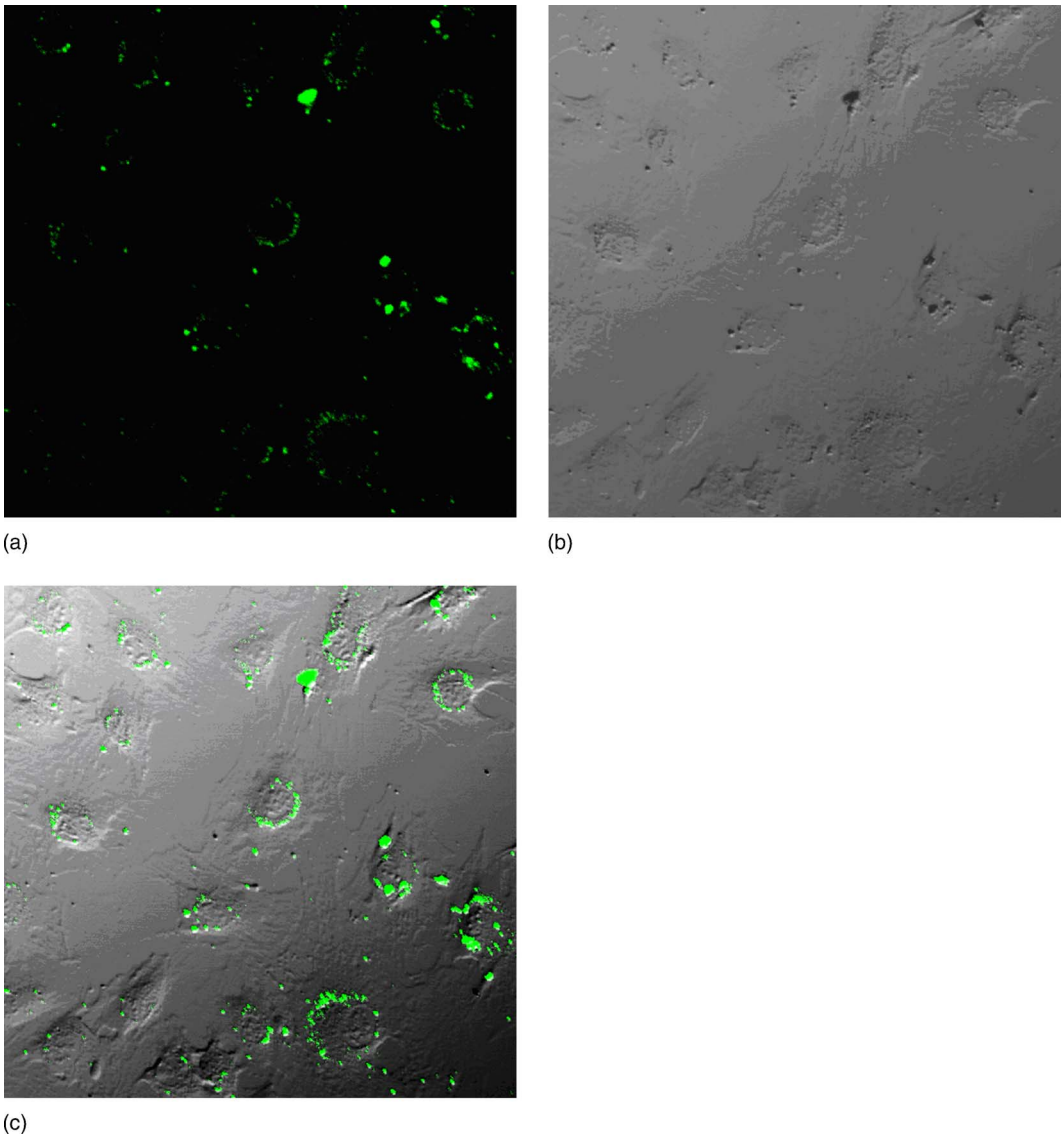

Fig. 9 PEI-coated nanoparticle sensors delivered to human dermal fibroblasts: (a) confocal fluorescence image obtained by collecting 520 to 600-nm emission due to 488-nm excitation, (b) Nomarski phase contrast transmission image of HDFs using a 488-nm laser, and (c) overlay of fluorescence and phase images.

the contribution to the 515-nm intensity from the source and ruthenium was found to be negligible. Thus, the fluorescence ratios were recalculated after subtracting 0.175 from the normalized intensity at 614 nm. Following this adjustment, the Stern-Volmer curve was found to be highly linear (R^2 =0.9996) with a quenching constant of K_{SV}=1.06/mM. Because of this excellent fit, consideration of more complex (e.g., two-state[29,46]) models for the system behavior was not necessary. Additionally, by applying this correction factor, the new sensitivity for the system was calculated to be S=60%, an improvement in apparent sensitivity of more than 30%. Thus, removal of the static spectral overlap due to the reference emission and source-specific offset value reveals that the indicator, immobilized on fluorescent templates in a facile manner within a self-assembled nanofilm, is in an environment that provides sensitivity similar to that observed for more complex approaches.[9,43]

The sensitivity of the system to the biological environment is also worthy of consideration. The results of comparative quenching experiments with and without poly(lysine) present [Fig. 8(b)] suggest minimal interference by the ambient peptide. The first-order coefficient for the power-law curve was identical, while the second-order coefficient decreased by approximately 30%. Similar results were observed for nanosensors in solution containing serum proteins; the emission spectra were slightly altered, but the Stern-Volmer plots were nearly identical to that calculated for the sensors with and without poly(lysine). The low susceptibility of the sensors to the presence of peptide/protein is likely because the dye is mainly buried beneath an outer layer of poly(ethyleneimine) that was applied after adsorption of the dye. Note also that the sensors used for these experiments [Fig. 8(b)] came from a different batch of sensors than those in the initial oxygen sensitivity experiments [Figs. 7, and 8(a)], where different rela-

tive concentrations of ruthenium to nanoparticles were used; therefore, the curves in the inset should be compared directly to one another, but not to the curve in the main figure.

3.4 *Intracellular Delivery*

Representative confocal fluorescence microscope and Nomarski phase images of PEI-coated nanoparticle sensors in human dermal fibroblasts are shown in Fig. 9. After a 48-h exposure, it was observed that a large fraction of nanoparticles were endocytosed by cells prior to rinsing. After washing with HBSS, noninternalized particles were removed and all remaining particles appeared to remain localized within the intracellular space. In many cases, the particles were not uniformly distributed in the cytoplasm, but rather became congregated in the perinuclear region. The human dermal fibroblasts remained viable, as determined with a propidium iodide test, and continued to grow and divide at consistent rates for 2 weeks following nanosensor introduction. The cells were passaged multiple times using standard techniques, and no deleterious effects of the nanosensors were observed. These findings indicate that internalization of PEI-coated nanosensors does not negatively interfere with cellular functions.

4 Conclusions

A method for adsorption of chromophore $[Ru(Ph_2phen)_3]^{2+}$ into electrostatically assembled films was elaborated for the application to sensor fabrication. Adsorption of $[Ru(Ph_2phen)_3]^{2+}$ was found to be nonlinear with respect to nanofilm thickness when deposited on planar surfaces with negative charge, whereas adsorption was negligible for positively charged surfaces. A novel sensor design using fluorescent particles as templates and references for fluorescence sensing was then evaluated, with the important characteristic of localization of fluorescence chemistry within polyelectrolyte nanofilms. These films, which offer a potential barrier to minimize problems traditionally associated with fluorescence sensor assays, specifically cytotoxicity and biofouling, are easily deposited under mild conditions and can be "tuned" in their properties and composition to realize specific functional characteristics. The sensors fabricated in this manner have been shown to be stable in aqueous solution for a period of 28 days; furthermore, they are easily dispersed and still exhibit similar sensitivity to oxygen following >10 months wet storage.

The design was analyzed in the context of oxygen sensing, based on the quenched fluorescence of $[Ru(Ph_2phen)_3]^{2+}$, from which is was found that the sensor response matches the linear Stern-Volmer equation. Response of the nanosensors to changes in oxygen concentration indicates that oxygen is transported through the films and that $[Ru(Ph_2phen)_3]^{2+}$ sensitivity to oxygen is not completely lost when adsorbed into polyelectrolyte multilayers; though a subpopulation of the adsorbed dye is only weakly quenched, these nanosensors exhibit a sensitivity that is similar to that observed for other systems, and it is anticipated that sensitivity can be optimized by selection of alternate nanofilm materials and adsorption conditions. Spectral overlap could be minimized by choice of a different reference fluorophore or longer wavelength indicators. The sensors were also successfully delivered to the interior of human dermal fibroblasts via a simple chemically induced endocytosis method utilizing an electrostatically adsorbed PEI coating on the sensor surface. Cells loaded with this method maintained viability and typical proliferative behavior after particle uptake.

This paper demonstrated the fabrication, oxygen sensitivity (in solution), and intracellular uptake of the sensors, but tests for intracellular application to validate the sensor function in the intended application are not included in this paper. Intracellular oxygen imaging is currently being developed using simultaneous two-wavelength video microscopy imaging applied to well- controlled culture conditions. Results from real-time intracellular oxygen measurements using the designed nanosensors will be the subject of future reports.

Acknowledgments

The authors gratefully acknowledge financial support from LaSPACE/National Aeronautics and Space Administration (NASA), NGT5-40115. We also thank Dr. Patrick Grant of Aura Nanotechnology for helpful discussions. Dr. Jim Spaulding and Dr. Debasish Kuila, along with LEO Electron Microscopes Division, are acknowledged for TEM imaging.

References

1. J. R. Lakowicz, *Principles of Fluorescence Spectroscopy*, 2nd ed., Kluwer/Plenum, New York, (1999).
2. R. J. Russell, M. V. Pishko, C. C. Gefrides, M. J. McShane, and G. L. Cote, "A fluorescence-based glucose biosensor using concanavalin A and dextran encapsulated in a poly(ethylene glycol) hydrogel," *Anal. Chem.* **71** (15), 3126–3132 (1999).
3. R. Ballerstadt and J. S. Schultz, "A fluorescence affinity hollow fiber sensor for continuous transdermal glucose monitoring," *Anal. Chem.* **72** (17), 4185–4192 (2000).
4. K. P. McNamara and Z. Rosenzweig, "Dye-encapsulating liposomes as fluorescence-based oxygen nanosensors," *Anal. Chem.* **70** (22), 4853–4859 (1998).
5. H. A. Clark, M. Hoyer, M. A. Philbert, and R. Kopelman, "Optical nanosensors for chemical analysis inside single living cells. 1. Fabrication, characterization, and methods for intracellular delivery of PEBBLE sensors," *Anal. Chem.* **71** (21), 4831–4836 (1999).
6. H. A. Clark, R. Kopelman, R. Tjalkens, and M. A. Philbert, "Optical nanosensors for chemical analysis inside single living cells. 2. Sensors for pH and calcium and the intracellular application of PEBBLE sensors," *Anal. Chem.* **71** (21), 4831–4836 (1999).
7. M. Brasuel, R. Kopelman, T. J. Miller, R. Tjalkens, and M. A. Philbert, "Fluorescent nanosensors for intracellular chemical analysis: decyl methacrylate liquid polymer matrix and ion-exchange-based potassium PEBBLE sensors with real-time application to viable rat C6 glioma cells," *Anal. Chem.* **73** (10), 2221–2228 (2000).
8. S. Santra, K. Wang, R. Tapec, and W. Tan, "Development of novel dye-doped silica nanoparticles for biomarker application," *J. Biomed. Opt.* **6** (2), 160–166 (2001).
9. H. Xu, J. W. Aylott, R. Kopelman, T. J. Miller, and M. A. Philbert, "A real-time ratiometric method for the determination of molecular oxygen inside living cells using sol-gel-based spherical optical nanosensors with applications to rat C6 glioma," *Anal. Chem.* **73**, 4124–4133 (2001).
10. Y. -E. L. Koo, Y. Cao, R. Kopelman, S. M. Koo, M. Brasuel, and M. A. Philbert, "Real-time measurements of dissolved oxygen inside live cells by organically modified silicate fluorescent nanosensors," *Anal. Chem.* **76**, 2498–2505 (2004).
11. G. Decher, "Fuzzy nanoassemblies: toward layered polymeric multicomposites," *Science* **277** (5330), 1232–1237 (1997).
12. Y. M. Lvov, G. Decher, and H. Mohwald, "Assembly, structural characterization, and thermal behavior of layer-by-layer deposited ultrathin films of poly(vinyl sulfate) and poly(allylamine)," *Langmuir* **9** (2), 481–486, (1993).
13. G. Decher and J. B. Schlenoff, *Multilayer Thin Films*, Chap. 1, Wiley-VCH, Weinheim (2003).

14. D. Yoo, S. Shiratori, and M. Rubner, "Controlling bilayer composition and surface wettability of sequentially adsorbed multilayers of weak polyelectrolytes," *Macromolecules* **31** (13), 4309–4318 (1998).
15. J. B. Schlenoff and S. T. Dubas, "Mechanism of polyelectrolyte multilayer growth: charge overcompensation and distribution," *Macromolecules* **34** (3), 592–598 (2001).
16. G. B. Sukhorukov, E. Donath, S. Davis, H. Lichtenfeld, F. Caruso, V. I. Popov, and H. Mohwald, "Stepwise polyelectrolyte assembly on particle surfaces—a novel approach to colloid design," *Int. Symp. Polym. Adv. Technol.* **9** (10–11), 759–767 (1998).
17. F. Caruso, R. A. Caruso, and H. Mohwald, "Nanoengineering of inorganic and hybrid hollow spheres by colloidal templating," *Science* **262** (5391), 1111–1114 (1998).
18. Y. Lvov, R. Price, A. Singh, J. Selinger, M. Spector, and J. Schnur, "Imaging nanoscale patterns on biologically derived microstructures," *Langmuir* **16** (14) 5932–5935 (2000).
19. J. Q. Brown and M. J. McShane, "Nanoengineered poly electrolyte micro- and nano-capsules as fluorescent potassium ion sensors," *IEEE EMBS Mag.* **22**, 118–123 (2003).
20. S. H. Lee, J. Kumar, and S. K. Tripathy, "Thin film optical sensors employing polyelectrolyte assembly," *Langmuir* **16** (26), 10482–10489 (2000).
21. P. S. Grant and M. J. McShane, "Development of multilayer fluorescent thin film chemical sensors using electrostatic self assembly," *IEEE Sens. J.* **3**, 139–146 (2003).
22. T. A. Duchesne, J. Q. Brown, K. B. Guice, Y. M. Lvov, and M. J. McShane, "Encapsulation and stability properties of nanoengineered polyelectrolyte capsules for use as fluorescent sensors," *Sens. Mater.* **14**, 293–308 (2002).
23. M. J. McShane, J. Q. Brown, K. B. Guice, and Y. M. Lvov, "Polyelectrolyte microshells as carriers for fluorescent sensors: loading and sensing properties of a ruthenium-based oxygen indicator," *J. Nanosci. Nanotechnol.* **2**, 411–416 (2002).
24. C. Tedeschi, F. Caruso, H. Mohwald, and S. Kirstein, "Adsorption and desorption behavior of an anionic pyrene chromophore in sequentially deposited polyelectrolyte-dye thin films," *J. Am. Chem. Soc.* **122** (24), 5841–5848 (2000).
25. S. Das and A. Pal, "Layer-by-layer self-assembling of a low molecular weight organic material by different electrostatic adsorption processes," *Langmuir* **18** (2), 458–461 (2002).
26. D. A. Chang-Yen, Y. M. Lvov, M. J. McShane, and B. K. Gale, "Electrostatic self-assembly of a ruthenium-based oxygen sensitive dye using polyion-dye interpolyelectrolyte formation," *Sens. Actuators, A* **87** (2), 336–345 (2002).
27. M. A. Saarinen, J. S. Reece, M. A. Arnold, and D. W. Murhammer, "Monitoring and controlling the dissolved oxygen (DO) concentration within the high aspect ratio vessel (HARV)," *Biotechnol. Prog.* **19** (4), 1335–1341 (2003).
28. L. Lamboursain, F. St.-Onge, and M. Jolicoeur, "A lab-built respirometer for plant and animal cell culture," *Biotechnol. Prog.* **18** (6), 1377–1386 (2002).
29. E. R. Carraway, J. N. Demas, B. A. DeGraff, and J. R. Bacon, "Photophysics and photochemistry of oxygen sensors based on luminescent transition-metal complexes," *Anal. Chem.* **63**, 337–342 (1991).
30. L. Li and D. R. Walt, "Dual-analyte fiber-optic sensor for the simultaneous and continuous measurements of glucose and oxygen," *Anal. Chem.* **59**, 2780–2785, (1987).
31. J. N. Demas and B. A. DeGraff, "Design and applications of highly luminescent transition metal complexes," *Anal. Chem.* **63**, 829A–837A (1991).
32. L. Sacksteder, J. N. Demas, and B. A. DeGraff, "Long lived, highly luminescent rhenium(I) complexes as molecular probes: intra- and intermolecular excited state interactions," *J. Am. Chem. Soc.* **115**, 8230–8238 (1993).
33. W. Xu, R. Schmidt, M. Whaley, J. N. Demas, B. A. DeGraff, E. K. Karikari, and B. L. Famer, "Oxygen sensors based on luminescence quenching: interactions of pyrene with the polymer supports," *Anal. Chem.* **67**, 3172–3180 (1995).
34. I. Klimant and O. S. Wolfbeis, "Oxygen-sensitive luminescent materials based on silicone-soluble ruthenium diimine complexes," *Anal. Chem.* **67** (18), 3160–3166 (1995).
35. I. L. Radtchenko, G. B. Sukhorukov, and H. Mohwald, "A novel method for encapsulation of poorly water-soluble drugs: precipitation in polyelectrolyte multilayer shells," *Int. J. Pharm.* **242** (1–2), 219–223 (2002).
36. M. Fang, P. S. Grant, M. J. McShane, G. B. Sukhorukov, V. Golub, and Y. M. Lvov, "Magnetic bio/nanoreactor with multilayer shells of glucose oxidase and inorganic nanoparticles," *Langmuir* **18** (16), 6338–6344 (2002).
37. E. W. Stein and M. J. McShane, "Multilayer lactate oxidase shells on colloidal carriers as engines for nanosensors," *IEEE Trans. Nanobiosci.* **3**, 133–137 (2003).
38. M. J. McShane, "Potential for glucose monitoring with nanoengineered fluorescent biosensors," *Diabetes Technol. Therapeut.* **4**, 533–538 (2002).
39. C. C. Berry, S. Rudershanusen, J. Teller, and A. S. G. Curtis, "Influence of elastin-coated 520 nm and 20 nm diameter nanoparticles on human fibroblasts *in vitro*," *IEEE Trans. Nanobiosci.* **1**, 105–109 (2002).
40. H. Ai, M. Fang, S. A. Jones, and Y. M. Lvov, "Electrostatic layer-by-layer nanoassembly on biological microtemplates: platelets," *Biomacromolecules* **3** (3), 560–564 (2002).
41. T. Farhat, G. Yassin, S. T. Dubas, and J. B. Schlenoff, "Water and ion pairing in polyelectrolyte multilayers," *Langmuir* **15** (20), 6621–6623 (1999).
42. P. Lavin, C. McDonagh, and B. D. MacCraith, "Optimization of Ormosil films for optical sensor applications," *J. Sol-Gel Sci. Technol.* **13**, 641–645 (1998).
43. C. McDonagh, B. D. MacCraith, and A. K. McEvoy, "Tailoring of sol-gel films for optical sensing of oxygen in gas and aqueous phase," *Anal. Chem.* **70**, 45–50 (1998).
44. Z. J. Fuller, W. D. Bare, K. A. Kneas, W. -Y. Xu, J. N. Demas, and B. A. DeGraff, "Photostability of luminescent ruthenium(II) complexes in polymers and in solution," *Anal. Chem.* **75**, 2670–2677 (2003).
45. J. R. Bacon and J. N. Demas, "Determination of oxygen concentrations by luminescence quenching of a polymer-immobilized transition-metal complex," *Anal. Chem.* **67**, 3746–3752 (1995).
46. A. Mills, "Response characteristics of optical sensors of oxygen: models based on a distribution in τ_0 or k_q," *Analyst (Cambridge, U.K.)* **124**, 1301–1307 (1999).